Human Reproduction, Vol.37, No.3, pp. 411–427, 2022
Advance Access Publication on January 6, 2022 https://doi.org/10.1093/humrep/deab283

human reproduction

ORIGINAL ARTICLE *Embryology*

Metabolic state of human blastocysts measured by fluorescence lifetime imaging microscopy

Marta Venturas [1,2,*], Jaimin S. Shah [3,4], Xingbo Yang [1], Tim H. Sanchez [1], William Conway[1,5], Denny Sakkas [4,†], and Dan J. Needleman [1,5,6,†]

[1]Molecular and Cellular Biology and School of Engineering and Applied Sciences, Harvard University, Cambridge, MA, USA [2]Departament de Biologia Cellular, Fisiologia i Immunologia, Universitat Autònoma de Barcelona, Cerdanyola, Spain [3]Beth Israel Deaconess Medical Center, Harvard Medical School, Boston, MA, USA [4]Boston IVF, Waltham, MA, USA [5]Physics Department, Harvard University, Cambridge, MA, USA [6]Center for Computational Biology, Flatiron Institute, New York, NY, USA

*Correspondence address. Molecular and Cellular Biology and School of Engineering and Applied Sciences, Harvard University, 52 Oxford St., NW Building Room 358, Cambridge, MA 02138, USA. E-mail: martaventu22@gmail.com https://orcid.org/0000-0003-3977-0152

Submitted on July 27, 2021; resubmitted on October 27, 2021; editorial decision on December 20, 2021

STUDY QUESTION: Can non-invasive metabolic imaging via fluorescence lifetime imaging microscopy (FLIM) detect variations in metabolic profiles between discarded human blastocysts?

SUMMARY ANSWER: FLIM revealed extensive variations in the metabolic state of discarded human blastocysts associated with blastocyst development over 36 h, the day after fertilization and blastocyst developmental stage, as well as metabolic heterogeneity within individual blastocysts.

WHAT IS KNOWN ALREADY: Mammalian embryos undergo large changes in metabolism over the course of preimplantation development. Embryo metabolism has long been linked to embryo viability, suggesting its potential utility in ART to aid in selecting high quality embryos. However, the metabolism of human embryos remains poorly characterized due to a lack of non-invasive methods to measure their metabolic state.

STUDY DESIGN, SIZE, DURATION: We conducted a prospective observational study. We used 215 morphologically normal human embryos from 137 patients that were discarded and donated for research under an approved institutional review board protocol. These embryos were imaged using metabolic imaging via FLIM to measure the autofluorescence of two central coenzymes, nicotinamide adenine (phosphate) dinucleotide (NAD(P)H) and flavine adenine dinucleotide (FAD+), which are essential for cellular respiration and glycolysis.

PARTICIPANTS/MATERIALS, SETTING, METHODS: Here, we used non-invasive FLIM to measure the metabolic state of human blastocysts. We first studied spatial patterns in the metabolic state within human blastocysts and the association of the metabolic state of the whole blastocysts with stage of expansion, day of development since fertilization and morphology. We explored the sensitivity of this technique in detecting metabolic variations between blastocysts from the same patient and between patients. Next, we explored whether FLIM can quantitatively measure metabolic changes through human blastocyst expansion and hatching via time-lapse imaging. For all test conditions, the level of significance was set at $P < 0.05$ after correction for multiple comparisons using Benjamini–Hochberg's false discovery rate.

MAIN RESULTS AND THE ROLE OF CHANCE: We found that FLIM is sensitive enough to detect significant metabolic differences between blastocysts. We found that metabolic variations between blastocyst are partially explained by both the time since fertilization and their developmental expansion stage ($P < 0.05$), but not their morphological grade. Substantial metabolic variations between blastocysts from the same patients remain, even after controlling for these factors. We also observe significant metabolic heterogeneity within individual blastocysts, including between the inner cell mass and the trophectoderm, and between the portions of hatching blastocysts within and without the zona pellucida ($P < 0.05$). And finally, we observed that the metabolic state of human blastocysts continuously varies over time.

LIMITATIONS, REASONS FOR CAUTION: Although we observed significant variations in metabolic parameters, our data are taken from human blastocysts that were discarded and donated for research and we do not know their clinical outcome. Moreover, the embryos used in this study are a mixture of aneuploid, euploid and embryos of unknown ploidy.

[†]The last two authors are the senior authors.

WIDER IMPLICATIONS OF THE FINDINGS: This work reveals novel aspects of the metabolism of human blastocysts and suggests that FLIM is a promising approach to assess embryo viability through non-invasive, quantitative measurements of their metabolism. These results further demonstrate that FLIM can provide biologically relevant information that may be valuable for the assessment of embryo quality.

STUDY FUNDING/COMPETING INTEREST(S): Supported by the Blavatnik Biomedical Accelerator Grant at Harvard University. Becker and Hickl GmbH and Boston Electronics sponsored research with the loaning of equipment for FLIM. D.J.N. is an inventor on patent US20170039415A1.

TRIAL REGISTRATION NUMBER: N/A.

Key words: metabolism / human blastocysts / embryo assessment / non-invasive / fluorescence lifetime imaging microscopy / embryo development

Introduction

Mammalian preimplantation embryos undergo dynamic metabolic changes necessary to support distinctive developmental events (Gardner *et al.*, 2001; Leese, 2012, 2015). Early stages of preimplantation embryo development rely primarily on pyruvate for energy generation (Leese, 2015; Harvey, 2019). It was previously thought that once the embryo reached the eight-cell stage, the embryo underwent a metabolic switch and glycolysis became the predominant pathway for ATP production (Gardner *et al.*, 2011; Gardner and Harvey, 2015; Leese, 2015). However, a number of studies have shown that glucose does not only contribute to energy production in mouse embryos, but instead plays crucial signaling roles required for blastocyst formation and cell fate specification (Chi *et al.*, 2020; Saha *et al.*, 2020; Zhu and Zernicka-Goetz, 2020). Glucose is also partially converted to lactate, which is thought to facilitate different aspects of implantation, including tissue invasion, angiogenesis and modulation of the immune response (Gardner, 2015). In parallel, oxygen consumption increases at the blastocysts stage (Houghton *et al.*, 1996; Trimarchi *et al.*, 2000; Gardner, 2015). Proper metabolic function is essential for producing developmentally viable eggs and embryos (Van Blerkom *et al.*, 1995; Gardner *et al.*, 2011; Harvey, 2019), and impaired metabolic activity has been correlated with decreased developmental potential in mouse (Wakefield *et al.*, 2011; Harvey, 2019) and human embryos (Van Blerkom *et al.*, 1995; Wilding *et al.*, 2001; Harvey, 2019). Embryos with the highest developmental potential were found to have low amino acid turnover (Brison *et al.*, 2004) and low rates of oxygen consumption (Houghton *et al.*, 1996; Lopes *et al.*, 2010). These observations led to the 'Quiet embryo hypothesis' by Leese (2002), which proposes that embryos with a higher developmental capacity are characterized by a quieter metabolism rather than an active one, which is suggested to be linked with cellular or molecular damage (Baumann *et al.*, 2007; Leese, 2012). However, in apparent contradiction with this hypothesis, some studies indicate that pyruvate (Turner *et al.*, 1994) and glucose uptake (Gardner and Leese, 1987) levels are higher in embryos that develop successfully.

Blastomeres in preimplantation embryos are genetically, morphologically and metabolically heterogeneous. Metabolic heterogeneity between blastomeres is thought to be associated with either cell lineage specification (Chi *et al.*, 2020) or cellular stress (Brison *et al.*, 2004) as high levels of heterogeneity have been linked with developmental arrest (Sutton-McDowall *et al.*, 2017). Cellular stress may be associated with increased DNA damage (Sturmey *et al.*, 2008), which could be either a cause or a consequence of cell metabolic (dys)function. At the blastocyst stage, clear cellular differentiation already exists, with the apical trophectoderm (TE) and inner cell mass (ICM), which give rise to the placenta and fetus, respectively. Studies in mouse (Hewitson and Leese, 1993; Van Blerkom *et al.*, 1995; Houghton, 2006; Van Blerkom, 2011; Gardner and Harvey, 2015) and human embryos (Gardner and Harvey, 2015), have found differences in mitochondrial physiology and activity between cells in the TE and ICM.

Developing tools to select the best embryo to transfer has been a long term focus in IVF (Gardner *et al.*, 2000; Seli *et al.*, 2007; Urbanski *et al.*, 2008). Improved embryo selection would decrease the number of transfers a patient must undergo, which would in turn, reduce its economical and emotional cost (Gardner and Leese, 1987; Gerris *et al.*, 2004). Current selection methods primarily rely on embryo morphology assessments (Schoolcraft *et al.*, 1999). Blastocyst morphology grading is typically based on the expansion stage, the consistency of both the ICM and TE and the time to blastocyst formation since fertilization (Schoolcraft *et al.*, 1999). Despite its widespread use, embryo morphological assessments have limited predictive power, and the further disadvantage that they are unable to provide a direct measure of the physiology of the embryo (Wong *et al.*, 2014). Alternative embryo selection approaches include: invasive preimplantation genetic testing for aneuploidy, which is increasingly being used (Penzias *et al.*, 2018; Munné *et al.*, 2019; Patrizio *et al.*, 2019); time-lapse imaging (Coticchio *et al.*, 2018), which provides detailed information on developmental dynamics; and, more recently, artificial intelligence (Tran *et al.*, 2019). Additionally, several studies in mouse and human embryos showed a clear association between metabolic function and implantation potential (Gardner and Leese, 1987; Van Blerkom *et al.*, 1995; Gardner *et al.*, 2011; Ahlström *et al.*, 2013). Embryo morphology (Tejera *et al.*, 2012) and time to blastocyst formation (Jones *et al.*, 2001) have also been found to be linked with embryo metabolism. This suggests that measures of metabolism might provide a means to select high quality embryos for transfer, but approaches based on this premise have so far not been successful (Jones *et al.*, 2001; Thompson *et al.*, 2016).

Many approaches to study embryo metabolism hinge on either intracellular measurements (Alm *et al.*, 2005; Al-Zubaidi *et al.*, 2019) or quantification of metabolites in the spent media to detect the metabolic activity of the whole embryo (Gardner and Leese, 1987; Conaghan *et al.*, 1993; Urbanski *et al.*, 2008; Vergouw *et al.*, 2008;

Gardner *et al.*, 2011). These methods are often either invasive or require highly specialized skills to perform. Recently, non-invasive methods to measure intracellular metabolic activity of oocytes and embryos have also been pursued. Several endogenous molecules like NADPH, nicotinamide adenine dinucleotide (NADH) and flavine adenine dinucleotide (FAD+) are autofluorescent (Heikal, 2010). These molecules are electron carriers that play key roles in metabolic pathways, which makes them ideal candidates for characterizing cellular metabolism (Klaidman *et al.*, 1995; Dumollard *et al.*, 2004). The fluorescence spectra of NADH and NADPH are almost indistinguishable (Ghukasyan and Heikal, 2014), therefore the combined fluorescence of NADH and NADPH is often referred to as the NAD(P)H signal. NAD(P)H (Dumollard *et al.*, 2007, 2009) and FAD+ (Sutton-McDowall *et al.*, 2017; Santos Monteiro *et al.*, 2021) autofluorescence intensity can be used to measure switches in the metabolic state of cells throughout development.

Additional information on NAD(P)H and FAD+ can be obtained using fluorescence lifetime imaging microscopy (FLIM) (Becker, 2012). FLIM not only provides information on fluorescence intensity, but also gives information on the fluorescence lifetime, i.e. the time the fluorophores remain in their excited state. The fluorescence lifetimes of NAD(P)H and FAD+ depend on their microenvironment, including their engagement with enzymes, and thus provides a sensitive means to characterize variations in metabolic state (Ghukasyan and Heikal, 2014). FLIM enables non-invasive, quantitative measurements of the metabolic state of mouse embryos (Sanchez *et al.*, 2018, 2019; Ma *et al.*, 2019), but its application to human preimplantation embryos has yet to be established (Cinco *et al.*, 2016). FLIM can be performed with two-photon fluorescence microscopy (Becker, 2005, 2012), which allows intrinsic sectioning and deep imaging (Mertz, 2019). Another advantage of performing FLIM with two-photon microscopy is that it enables simultaneous non-invasive imaging of spindle morphology via second-harmonic generation (SHG). SHG is a non-linear phenomenon that occurs when light scatters from highly ordered structures that lack inversion symmetry, like the spindle (Hsieh *et al.*, 2008; Yu *et al.*, 2014; Mertz, 2019; Sanchez *et al.*, 2019). The use of non-invasive FLIM in combination with SHG has been previously described in mouse embryos (Sanchez *et al.*, 2019). However, its utility for studying preimplantation human embryos has not been demonstrated. A key question is: is this technique sensitive enough to measure the metabolic differences that occur within and between human embryos? Non-invasive techniques to simultaneously measure the cellular metabolic state and spindle dynamics of human embryos can offer a better understanding of basic embryo biology and may assist in improving embryo screening in a clinical setting.

In this study, we used non-invasive FLIM to measure the metabolic state of human blastocysts. First, we studied spatial patterns in the metabolic state within human blastocysts and the association of embryo metabolic state with the stage of expansion, day of development since fertilization and morphology. Second, we show that this technique is sensitive enough to resolve the metabolic variations between blastocysts from the same patient and between patients. Last, we explored the extent to which time-lapse FLIM imaging can quantitatively measure metabolic changes through human blastocyst expansion and hatching.

Materials and methods

Sample preparation

Human blastocysts were discarded and donated for research under determinations by the Beth Israel Deaconess Medical Center and New England institutional review boards (New England IRB WO 1-6450-1). A total of 215 vitrified human blastocysts from 137 patients, with a mean ± standard deviation age of 35.4 ± 4.7 years, BMI of 25.9 ± 5.2 kg/m^2 and mean anti-Müllerian hormone (AMH) of 3.55 ± 2.9 ng/ml were analyzed in this experiment. These embryos were thawed according to the manufacturer's recommendations (90137-SO—Vit Kit-Thaw, FUJIFILM Irvine Scientific, USA) and cultured for 2 h in individual drops of 50 µl of Continuous Single Culture Complete (CSC) media with human serum albumin media (HSA) (FUJIFILM Irvine Scientific, USA) overlain with mineral oil in an incubator at 37 °C, 7% CO_2 and 6% O_2. Patient clinical characteristics, such as age, BMI and AMH hormone levels were provided in a de-identified database. Blastocyst's morphological grades (Schoolcraft *et al.*, 1999) were evaluated at the time of imaging by a senior embryologist. An ICM and TE grade A, B or C was assigned for each blastocyst. Stage of development (early, expanded, hatching or hatched blastocyst) and day since fertilization (Day 5 or 6) was also monitored for each embryo.

For the blastocyst development time-lapse imaging experiment, 17 human blastocysts from 17 different patients were analyzed. Blastocyst's morphological grade was assessed before and after the 36 h time-lapse experiment.

Imaging protocols

Discarded blastocysts were transferred and imaged in a custom glass-bottomed microwell dish with 80 µl of media overlain with mineral oil, in an on-stage incubation system (Ibidi GmbH, Martinsried, Germany) to maintain environmental culture conditions of 37 °C, 7% CO_2 and 6% O_2.

For the single time-point blastocyst experiment, FLIM images were taken once 2 h after thawing at three *Z*-planes 7 um apart, using 12 mW for NAD(P)H and 20 mW for FAD+ and 60 s of integration time for each plane.

For the blastocyst development time-lapse experiment, we compared the results from two different protocols. Two hours after thawing embryos: (i) for 10 human blastocysts, metabolic measurements were taken every 2 h over the course of 36 h (at three *Z*-planes 7 um apart) using the same parameters as explained above for each plane; (ii) for seven human blastocysts, one metabolic measurement was taken (at three *Z*-planes 7 um apart), and the embryos were incubated on the microscope without further exposure to illumination for 36 h. For all 17 blastocysts, a final metabolic image was taken after 36 h on the microscope.

Staining protocols

For MitoTraker experiments, five blastocysts were incubated with 5 nM MitoTraker Red CMXRos (M7512, Thermo Fisher, USA) for 20 min. For DNA staining experiments, five embryos were stained with 1 ug/ml of Hoechst (Thermo Fisher, USA) for 20 min. The

samples were then washed three times in CSC + HSA and transferred to a glass bottom dish for imaging.

Fluorescence lifetime imaging microscopy

FLIM measurements were performed on a Nikon TE300 (Nikon, Japan) microscope using two-photon excitation from a Ti: Sapphire pulsed laser (M-squared Lasers, UK) with a 80 MHz repetition rate and 150 fs pulse width, a galvanometric scanner, time-correlated single-photon counting module (SPC-150, Becker and Hickl, Germany) and a hybrid single-photon counting detector (HPM-100-40, Becker and Hickl, Germany). Imaging was performed with a 20× Nikon objective with 0.75 numerical aperture (CFI Apo 20×, NA 0.75, Nikon). The wavelengths of NAD(P)H and FAD+ excitation were set to 750 and 890 nm, respectively. The power output was measured through the objective in the sample plane with a handheld power meter (Thorlabs, USA). The corresponding powers measured at the sample plane used were 12 mW for NAD(P)H and 20 mW for FAD+. Optical bandpass filters were positioned in a filter wheel in front of the detector—447 ± 30 nm bandwidth for NAD(P)H (BrightLine, Semrock, USA) and 550 ± 44 nm bandwidth for FAD+ (Chroma technologies) with an additional 650 nm short-pass filter mounted on the detector (Chroma technologies). SHG was detected simultaneous with FAD imaging by a single-photon counting detector (PMC-150, Becker-Hickl GmbH, Germany) in the forward direction, with 650 short-pass and 440 ± 10 nm bandwidth bandpass filters (BrightLine, Semrock, USA). Each NAD(P)H and FAD+ image was acquired with 60 s of integration time. A customized motorized stage (using CONEX TRA12CC actuators, Newport, USA) was used to perform multi-dimensional acquisitions. We acquired three FLIM images varying Z axis per each human blastocyst. All the electronics were controlled by SPCM software (Becker and Hickl, Germany) and custom LabVIEW software.

Data analysis

Data were analyzed using a custom code written in MATLAB version R2019b (MathWorks, USA). Samples were incorporated to the analysis according to the information available. NAD(P)H and FAD+ images were trained using a supervised machine-learning segmentation software (Illastik, version 1.0 (Berg *et al.*, 2019)) to classify pixels in intensity images into either NAD(P)H or FAD+ signal from the cells or the background. The algorithm was trained using 40 random NAD(P)H and FAD+ intensity images. For each cell segment, the photon arrival time histogram was modeled as a bi-exponential decay:

$$P(t) = A[(1 - F) \times e^{(-t/\tau_1)} + F \times e^{(-t/\tau_2)}] + B$$

Where, A is a normalization factor, B is the background, τ_1 is the short lifetime, τ_2 is the long lifetime and F is the fraction of molecule with long lifetime (fraction engaged with enzymes for NAD(P)H and unengaged for FAD+). This function was convolved with a measured instrument response function to model the experimental data, and the least square fitting yielded quantitative values for these fit parameters. The fluorescence intensity was calculated for each embryo dividing the number of photons by the area of the embryo. An additional parameter, the redox ratio (NAD(P)H fluorescence intensity/FAD+ fluorescence intensity) was also calculated per image. Together, a single FLIM measurement produced nine parameters, four for NAD(P)H and four for FAD+ and redox ratio, to quantitatively characterize the metabolic state of human blastocysts.

The average photon arrival time of NAD(P)H and FAD+ was computed for each pixel within the embryo by averaging over the directly measured photon arrival time of all photons coming from NAD(P)H and FAD+ within a single pixel. Since the single pixel average is noisy due to limited photon counts per pixel, we smoothened the data by averaging each pixel over its neighboring pixels weighted by a Gaussian kernel with a 20 pixel standard deviation. We only averaged over pixels within the embryo and excluded pixels of the background and the cavity of the embryo. As a statistical control, we randomized the photon arrival times in each pixel by drawing a random photon arrival time from a Gaussian distribution with a mean of the average photon arrive time and a variance equal to that of the photon arrival time distribution of the blastocyst. This procedure produces a randomized photon arrival time image of the blastocyst with the exact same geometry. We repeated the average photon arrival time calculation described above for this 'control image' to test if there was any artifact associated with the averaging procedure. The control image consistently produced a homogeneous average photon arrival time, suggesting the heterogeneity observed in the blastocyst is of a biological origin rather than statistical artifact.

Statistical analysis

All statistical tests were performed using Stata Statistical Software version 16.0 (LLC Stata Corp, TX, USA) and R Studio Version 1.3.959 (R Foundation for Statistical Computing, Vienna, Austria). Our data were structured hierarchically, three images per embryo (i) and 1–7 embryos (j) per patient (k). Therefore, we used multilevel models with restricted maximum likelihood estimates (Snijders and Bosker, 2011) to analyze this structured data. We incorporated the corresponding predictors (embryo morphology, day, expansion stage or patient age, BMI and AMH) for each analysis, using the multilevel model:

$$\text{FLIMparam}_{ijk} = \beta_0 + \beta_1 \times \text{embryo characteristics} + c_{0,k} + b_{0,jk} + e_{ijk}$$

Where β_0 corresponds to the intercept; β_1 to the slope; embryo characteristics to the day, stage or morphological grading of the embryos; $c_{0,k}$ is the patient level random error; $b_{0,jk}$ is the embryo level random error; and e_{ijk} is the image random error (Snijders and Bosker, 2011). This modeling encodes information on the variance associated with each level: patient, embryos within patients and images within an embryo. One tailed Z-test was performed to determine whether these variances were significantly different than zero. The described experiments were performed by two different operators. Controlling for the operator in the multilevel model did not impact the results.

Additionally, paired t-tests were performed to detect metabolic variations between the ICM and the TE of each embryo. For all comparisons of ratios, one sample t-test was performed to determine whether these ratios were significantly different than one. Furthermore, we calculated the percentage change of all metabolic parameters between each expansion stage compared to the early blastocyst stage and pairwise comparisons were performed to analyze their significance. All P-values were corrected for multiple comparisons

using Benjamini–Hochberg's false discovery rate (FDR), at a q value of 0.05. FDR P-values of <0.05 were considered statistically significant.

We used a support vector machine (SVM) algorithm (Cristianini and Shawe-Taylor, 1999) to fit a hyperplane that best separates Days 5 and 6 embryos. All the data were randomly divided into two sets, a training set (70%) and a test set (30%). We performed SVM on the training set, and then we tested the accuracy of this model using the test set.

Furthermore, to understand the conditional dependencies between embryo day, expansion stage and the metabolic parameters, we constructed probabilistic graphical models (Neapolitan, 2009; Pearl, 2016) using standardized embryo metabolic parameters ($\frac{x-\text{mean}(x)}{\text{sd}}$), embryo day and stage. A directed arrow was drawn from variable a (embryo day) to variable b (embryo stage) if the probability distribution of a depends on b, and can be written as $P(a, b) = P(a)P(b|a)$. These conditional dependencies can be represented by a directed acyclic graph (DAG). We then computed the percentage of variance explained by both embryo day and stage for each level ($\frac{\text{Variance Patient Level}}{\text{Total Variance}}$ %), which can represent the effect size of the model (Lorah, 2018).

Finally, we calculated the percentage change of all metabolic parameters between embryos at Days 5 and 6 and between timepoint 0 and 24 h after time-lapse imaging. T-test with FDR correction was performed to analyze their significance.

Results

Two-photon microscopy of endogenous autofluorescence and SHG imaging enable visualization of subcellular structures in preimplantation human embryos

Preimplantation human embryos are often visualized using bright-field microscopy in IVF clinics, which is sufficient for blastocyst morphological grading but provides limited cellular and subcellular information (Fig. 1A). We first investigated what additional morphological information can be provided by two-photon microscopy of endogenous NAD(P)H and FAD+. Two-photon microscopy enables deep tissue imaging with optical sectioning (Mertz, 2019), allowing us to perform three dimensional (3D) reconstruction of blastocysts by combing multiple Z plane images of NAD(P)H autofluorescence (Fig. 1B). Cell nuclei appear as dark ovals in these 3D reconstructions (Fig. 1B, arrow), as confirmed by comparison to 3D reconstruction of human embryos stained for DNA with Hoechst (Fig. 1C). As FAD+ is significantly more enriched in mitochondria than NAD(P)H in many systems (Klaidman *et al.*, 1995; Dumollard *et al.*, 2004), we sought to determine the extent to which two-photon microscopy of FAD+ can provide information on mitochondrial localization in human preimplantation embryos. We stained five human blastocysts from five different patients with MitoTraker Red CMXRos, a dye that specifically labels mitochondria, and simultaneously imaged MitoTraker and FAD+ autofluorescence (Fig. 1D). We used machine-learning-based software (Illastik, version 1.0 (Berg *et al.*, 2019)) to segment bright intracellular regions in both the MitoTraker and FAD+ images and found an overlap of photons between regions of 89% ± 8%. Hence, the overwhelming majority of the FAD+ signal in human blastocyst is associated with mitochondria, and thus FAD+ imaging provides information on mitochondrial localization. The same laser illumination used for two-photon microscopy can be simultaneously employed for SHG, which we combined with FAD+ imaging, as previously described (Sanchez *et al.*, 2019). Using both autofluorescence and SHG imaging, it was possible to observe spindles in mitotic cells in all human blastocysts, along with the subsequent cell divisions (Fig. 1E, Supplementary Fig. S1 and Videos S1 and S2). Thus, two-photon microscopy of NAD(P)H and FAD+, combined with SHG imaging, provides a non-invasive means to image cellular and subcellular structures in human blastocysts, including mitochondria, nuclei and spindles.

To quantify the metabolic state of human blastocysts, we used an intensity-based machine-learning algorithm (see Materials and methods) to segment both the NAD(P)H (Fig. 1F and G, upper) and the FAD+ signal (Fig. 1F and G, lower). We then grouped all photons from the segmented regions to obtain histograms of NAD(P)H (Fig. 1H, upper) and FAD+ (Fig. 1H, lower) photon arrival times, which we fit using two-exponential decay models (Fig. 1H, black lines). This provided nine metabolic FLIM related parameters at each point in time: fluorescence intensity, short and long lifetimes and the fraction of molecules engaged with enzymes for both NAD(P)H and FAD+, as well as the redox ratio (NAD(P)H intensity/FAD+ intensity).

Spatial variation in human blastocysts metabolic parameters

We next imaged a total of 215 human blastocysts from 137 patients that were discarded and donated for research. FLIM data were taken at a single timepoint for each blastocyst, acquired 2 h after thawing.

We first used this data to investigate the spatial variation in metabolic parameters within human blastocysts. In the segmented the images, we calculated the average photon arrival time (see Materials and methods) and visualized the spatial distribution of average photon arrival times for NAD(P)H (Fig. 2A) and FAD+ (Fig. 2B), which appeared to indicate different metabolic signatures in the ICM and TE. These spatial patterns disappear after randomizing the photon arrival times for each pixel in the segmented region (Supplementary Fig. S2), indicating that the observed spatial patterns are real and not an artifact of the averaging procedure or the geometry of the blastocyst (Materials and methods). To further investigate the difference in metabolism between the ICM and TE, we manually segmented them and grouped photons from each region to determine their FLIM parameters (n = 187 from 125 patients). All metabolic parameters displayed significant differences between ICM and TE as measured by a paired t-test with *post-hoc* correction using Benjamini–Hochberg's FDR (FDR $P < 0.0001$). We were concerned that the different number of photons acquired from the two regions might artificially contribute to the measured difference in FLIM parameters. We therefore repeated the analysis, but by randomly selecting the same number of photons from the ICM and the TE. All the significant differences were upheld (FDR $P < 0.0005$), indicating that the measured difference in FLIM parameters is robust to the number of photons acquired. The observed differences in FLIM parameters between ICM and TE argue that cells in these regions are in different metabolic states (Fig. 2C). To further investigate this on the single embryo level, we calculated the ratio of each FLIM parameter between the ICM and TE of every embryo. While the average of each ratio across embryos was significantly

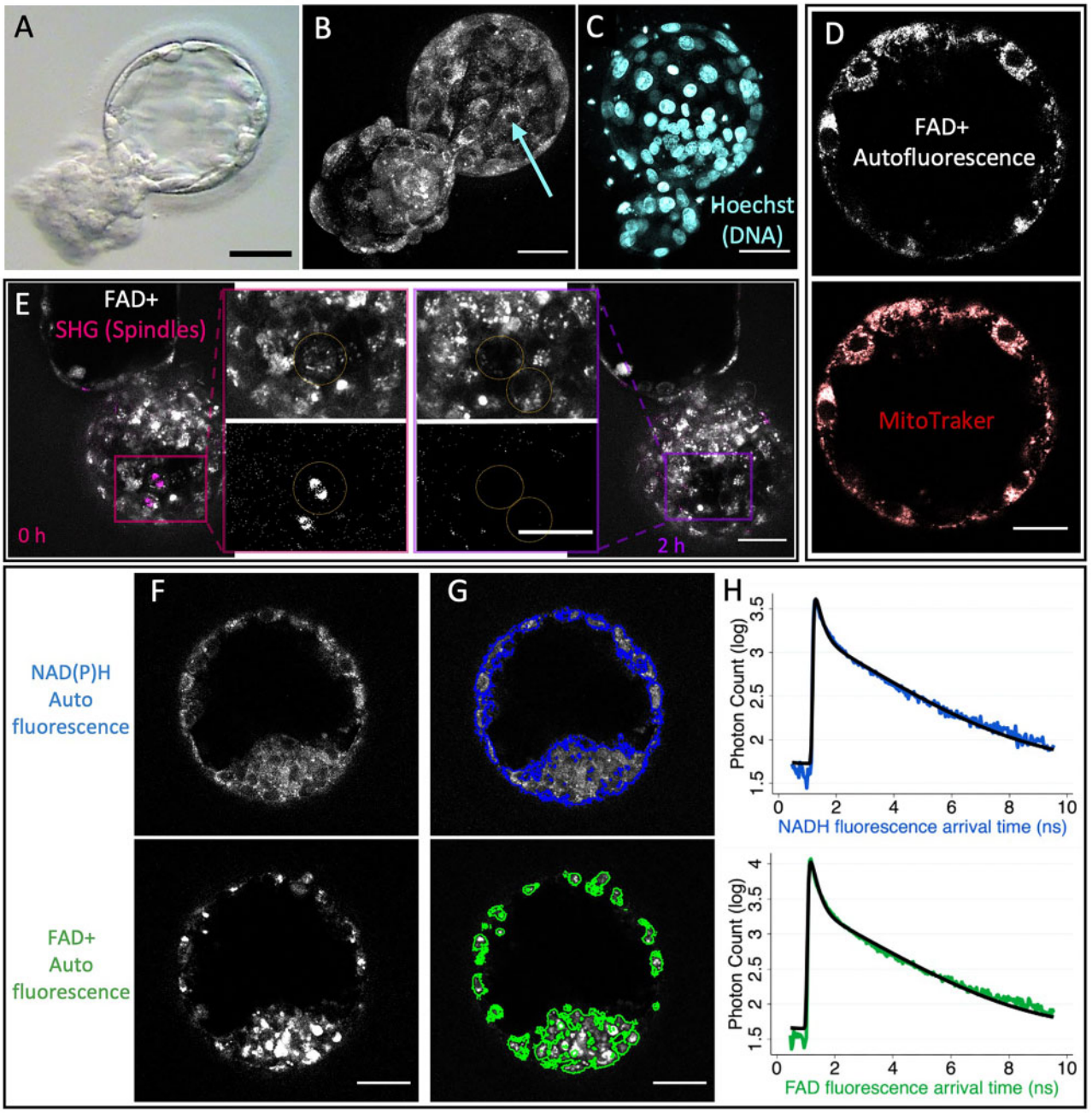

Figure 1. Two-photon fluorescence lifetime imaging microscopy (FLIM) and second-harmonic generation (SHG) enable visualization of cellular and subcellular structures. (**A**) Standard bright-field image of a human discarded blastocyst. (**B**) 3D reconstruction of two-photon NAD(P)H intensity images from multiple focal planes of the same blastocyst. Two-photon microscopy enables the detection of subcellular structures, such as the nucleus (blue arrow). (**C**) 3-D reconstruction of DNA staining Hoechst showing cell nuclei. (**D**) Simultaneous FLIM FAD+ autofluorescence of a human blastocyst and mitochondria dye, MitoTraker Red CMXRos, demonstrate a high colocalization. (**E**) SHG-spindle imaging (in magenta, false color), in combination with FLIM FAD+ autofluorescence imaging (in gray) enables detection of spindle formation capturing cellular mitotic divisions (also observed in Supplementary Fig. S1 and Videos S1 and S2). An overlap image of a human blastocyst of FAD+ autofluorescence in gray and mitotic spindle in magenta. Boxed regions show a zoom of the individual channels FAD+(top) and SHG-spindle imaging (bottom). At time 0 h (left), we observe a cell in mitosis highlighted with yellow circles with a spindle. This cell then divides into two cells at time 2 h (right). FLIM time-lapse imaging of the autofluorescence of NAD(P)H (**F**, top), and of FAD+ (F, bottom) of a human blastocyst. Supervised machine learning was applied to create masks to segment the fluorescence signal of NAD(P)H (**G**, upper) or FAD+ (G, lower). (**H**) All photon arrival times from a single embryo mask were combined to create a fluorescence decay for each fluorophore (NAD(P)H in blue and FAD+ in green). These curves were fitted to a two-exponential model (black curves) to obtain the quantitative parameters for characterizing the metabolic state of an embryo. Scale bars, 40 μm. FAD+, flavine adenine dinucleotide.

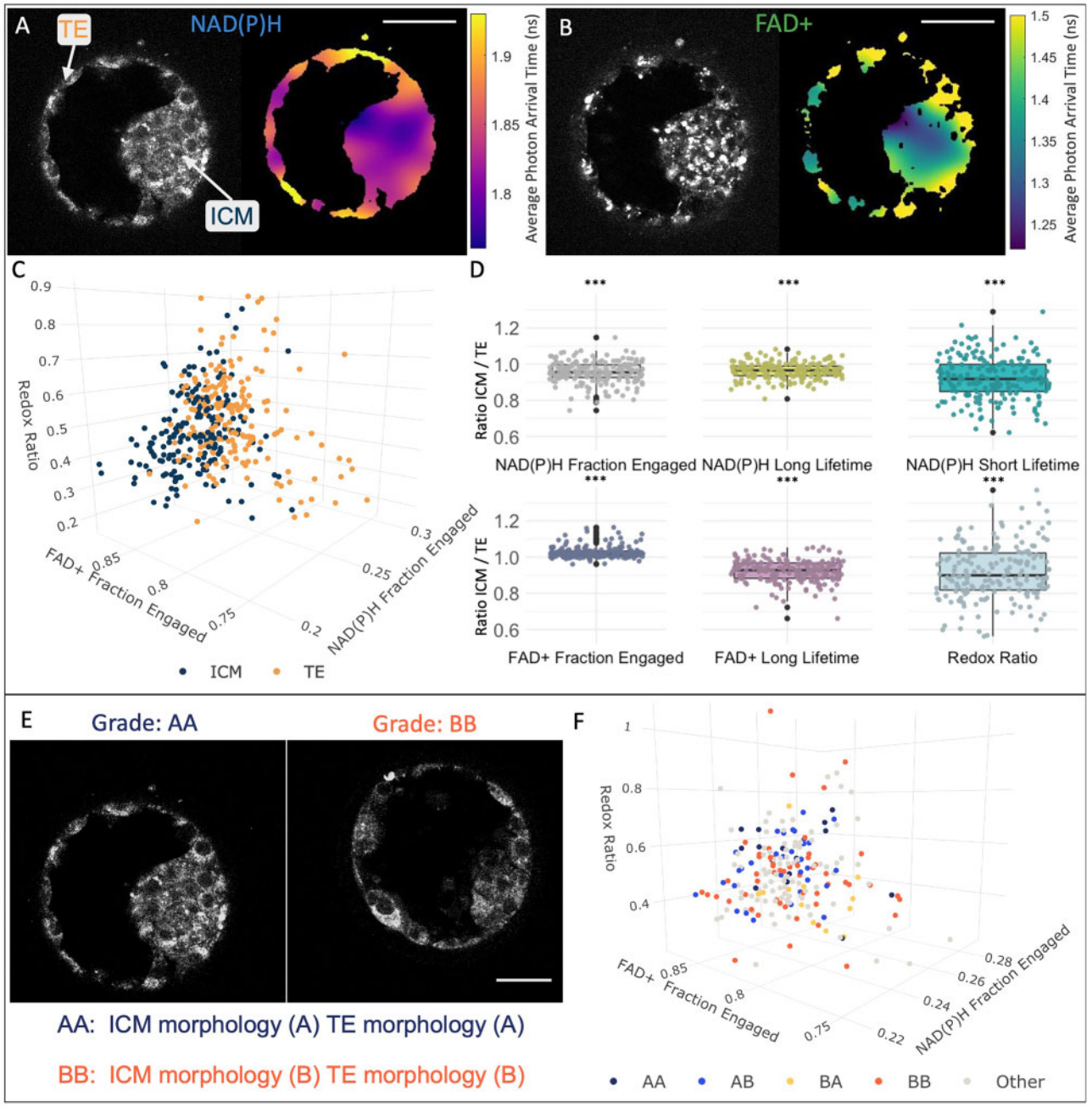

Figure 2. Variations in metabolic signatures between inner cell mass (ICM) and trophectoderm (TE) of human blastocysts. FLIM intensity image (left) and image of the average photon arrival time (right) of NAD(P)H (**A**) and of FAD+ (**B**) reveal spatial pattern of average photon arrival times, suggesting different metabolic state between the ICM and TE. Color bars show the average photon arrival times in nanoseconds. (**C**) FLIM parameters with the largest separation between ICM (blue) and TE (orange) were plotted in this 3D plot (n = 187 from 125 patients, false discovery rate (FDR) $P < 0.001$). Each dot corresponds to the mean of three Z images of the ICM or TE of single embryo. The fraction engaged corresponds to the fraction of these molecules that is engaged with enzymes. (**D**) Ratios of the FLIM parameters between the ICM and the TE. The box plots depict the interquartile range of the ratio, the center of the box represents the mean, the horizontal line in the box represents the median and the vertical lines represent the 5 and 95% quartiles. Black dots represent points outside of the interquartile range. Color dots represent the average ratio per each individual embryo. (**E**) Example of NAD(P)H intensity images of two human discarded blastocysts with varying morphological grading (AA and BB). (**F**) FLIM parameters were compared between blastocysts of different morphological categories: AA (n = 16 from 12 patients), AB (n = 32 from 32 patients), BA (n = 12 from 12 patients), BB (n = 55 from 48 patients) and other (n = 98 from 79 patients), this 3D plot shows no significant differences of metabolic signatures between embryo morphology grades (FDR $P > 0.05$). Each dot corresponds to the mean of an embryo. Scale bars, 40 μm. *** signifies FDR $P < 0.001$. FAD+, flavine adenine dinucleotide; FLIM, fluorescence lifetime imaging microscopy.

different from 1 (FDR $P < 0.0001$), there was substantial embryo-to-embryo variability (Fig. 2D).

We next explored if the embryo-to-embryo differences in FLIM of TE and ICM was related to the known large variations in TE and ICM morphology in human blastocysts. A senior embryologist graded the ICM and TE morphology of each embryo at the time of imaging using the standard grading system described by Schoolcraft *et al.* (1999). Briefly, an ICM with many, compacted cells are considered to be grade A, if it has several cells and they are loosely grouped, it is grade B, whereas if it contains very few cells, it is considered grade C. For the TE, a score A is assigned if the blastocyst has many cells that form a cohesive epithelium, if it has fewer cells, then it is graded as B, and if the TE has very few, large cells it is given a grade of C. These embryos then were divided into five categories: 16 embryos from 12 patients with grade AA, 32 from 32 patients with grade AB, 12 from 12 patients with BA, 55 from 48 patients with BB and 98 from 79 patients were categorized as other (any with C). The first and second letter corresponds to the ICM and TE grade, respectively. None of the FLIM parameters showed significant differences between morphological groups (FDR $P > 0.05$) (Fig. 2F). Thus, the embryo-to-embryo differences in FLIM of TE and ICM is not associated with variations in TE and ICM morphology.

Temporal variations of human blastocysts metabolic state

Blastocyst stage

To further study the metabolic shifts observed during blastocyst development, we explored the relationship between FLIM parameters, averaged over the entire embryo at a single timepoint, and embryo stage. A senior embryologist assigned each human discarded blastocyst to one of four stages (Fig. 3A): early blastocysts (n = 25 embryos from 25 patients), expanded blastocyst (n = 56 from 45 patients), hatching blastocyst (n = 101 from 74 patients) and fully hatched blastocyst (n = 31 from 29 patients). We computed the percentage relative to early blastocyst for each FLIM parameter and stage. FAD+ fraction engaged, FAD+ long lifetime, FAD+ short lifetime and redox ratio all exhibited significant variations (FDR $P < 0.001$), with the largest occurring for hatching and fully hatched blastocysts (Fig. 3B). We next investigated the potential existence of subtle changes in FLIM parameters during blastocysts expansion by testing for correlations between the diameter of early and expanding blastocysts with FLIM parameters. There were no significant correlations between these metabolic profiles and the diameter of the blastocysts (FDR $P > 0.05$). Thus, the largest changes in FLIM parameters are associated with the process of blastocyst hatching.

To better understand the metabolic variations associated with hatching, we examined the differences in FLIM parameters between the portions of TE inside the zona pellucida compared to those outside. We analyzed 36 hatching blastocysts from our cohort that had a substantial area both inside and outside the zona pellucida (Fig. 3C). We computed the ratio of FLIM parameters between the TE portion of the blastocyst inside and outside the zona pellucida. NAD(P)H intensity (FDR $P < 0.02$), fraction engaged (FDR $P < 0.02$), NAD(P)H long (FDR $P < 0.03$) and short lifetime (FDR $P < 0.03$), FAD+ fraction engaged (FDR $P = 0.03$), FAD+ short lifetime (FDR $P = 0.04$) and the redox ratio (FDR $P = 0.02$), all exhibit significant differences between the TE portion of the blastocyst inside and outside the zona pellucida (Fig. 3D).

Day of development since fertilization

The discarded human blastocysts we studied were vitrified at different periods of time after fertilization, the majority either on Day 5 (n = 98 embryos from 71 patients) or on Day 6 (n = 111 from 77 patients). We used multilevel models to compare FLIM parameters of Days 5 and 6 blastocysts. We found significant variations in NAD(P)H intensity (FDR $P = 0.002$), FAD+ intensity (FDR $P = 0.01$), FAD+ fraction engaged, FAD+ long and short lifetime and redox ratio (FDR $P < 0.0002$). The separation was so strong that a SVM generated hyperplane based on just three FLIM parameters gave predictions of whether an embryo was Day 5 or 6 with an accuracy of 77% (Fig. 3E).

Embryos develop to later stages over time, so, it would be possible that differences in FLIM parameters between Days 5 and 6 embryos might be due to embryos being at different developmental stages on these days. To investigate this, we explored the conditional dependencies between the day of embryo development since fertilization, stage of expansion and the FLIM parameters that were significantly associated with both of those (FAD+ fraction engaged, FAD+ long lifetime, FAD+ short lifetime and redox ratio). We began by investigating FAD+ short lifetime. Subdividing the embryos into two different stage categories (early/expanded or hatching/hatched) on both Days 5 and 6 demonstrates that day and stage both impact FAD+ short lifetime (Fig. 3F). Upon conditioning on stage of expansion, the partial correlation between day of embryo development and FAD+ short lifetime (day, FAD+ short lifetime | stage), is 0.53 ($P < 0.0001$). Upon condition on day of embryo development, the partial correlation between embryo stage of expansion and FAD+ short lifetime (stage, FAD+ short lifetime| day), is 0.39 ($P < 0.0001$). Thus, expansion stage and day of embryo development are both associated with FAD+ short lifetime. Furthermore, day of embryo development and expansion stage are correlated with a coefficient of 0.46 ($P < 0.00001$), after conditioning on FLIM parameters. These conditional dependencies can be represented by a DAG, which shows that day of embryo development, expansion stage and FAD+ short lifetime all depend on each other (Fig. 3G). Similar results held for the other FLIM parameters (Supplementary Fig. S3).

Metabolic variance between human blastocysts, between patients and between images

Embryo day of development and expansion stage are two factors which lead to differences in metabolism between different human preimplantation embryos. There are presumably other factors that also contribute to these differences. Some of these factors may cause differences in metabolism between embryos from different patients, whereas other factors may cause differences in metabolism between different embryos from the same patient. Indeed, plotting FLIM measurements from different embryos from the same patient often leads to a clear separation between embryos (Fig. 4A). In contrast, plotting FLIM parameters from embryos from different patients often produces substantial overlap (Fig. 4B). Thus, factors that produce differences in metabolism between embryos from different patients appear to be more subtle than the factors that produce variations between embryos from one

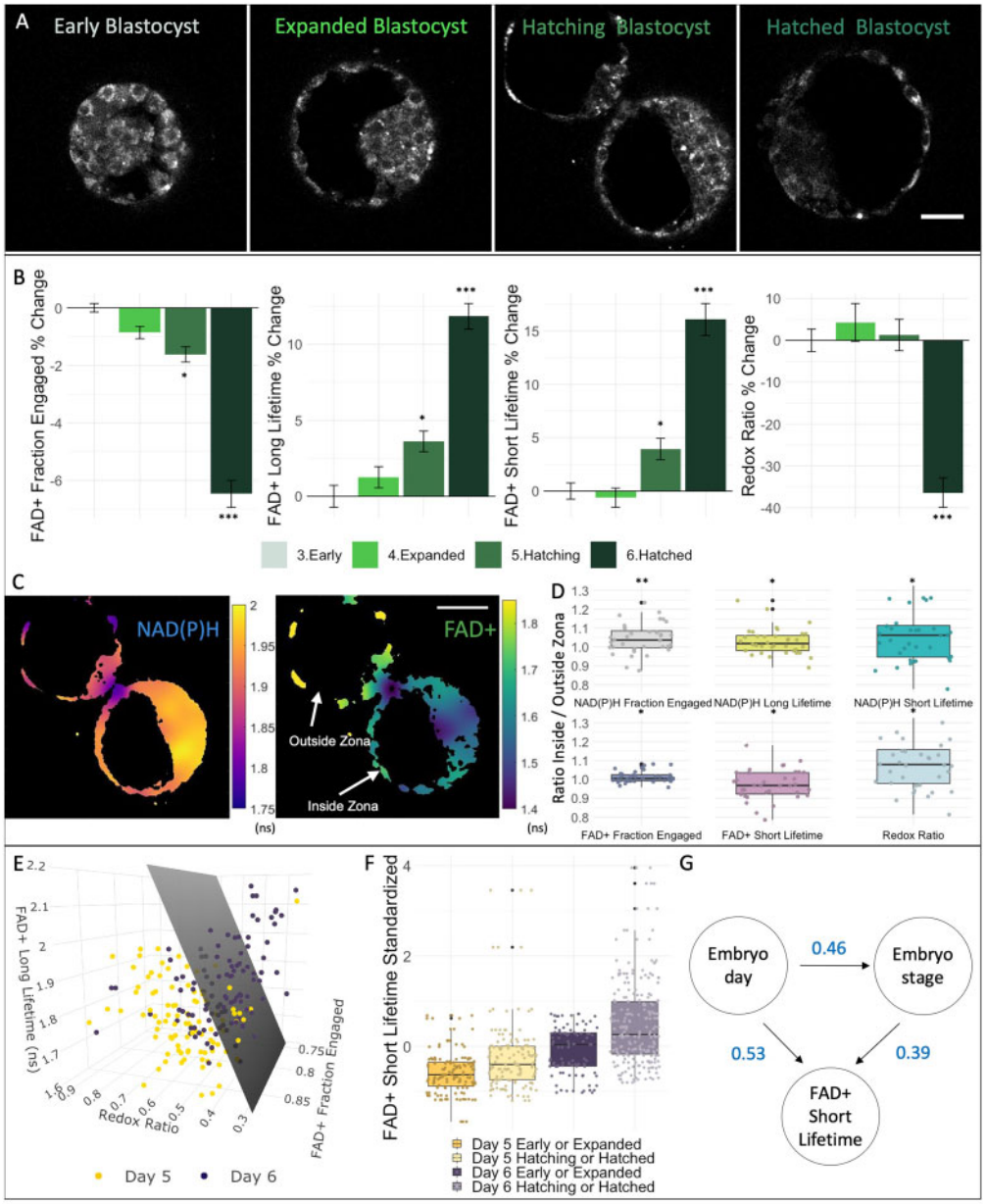

Figure 3. Human blastocyst metabolic state is associated with embryo day and embryo expansion stage. (**A**) NAD(P)H intensity images of four human blastocysts with varying expansion grade: early (n = 25 from 25 patients), expanded (n = 56 from 45 patients), hatching (n = 101 from 74 patients) and hatched (n = 31 from 29 patients) blastocysts. (**B**) Bar plots of the percentage change from early blastocysts of FAD+ fraction engaged, FAD+ long lifetime, FAD+ short lifetime and redox ratio with standard error bars displayed, showing a distinctive variation in these FLIM parameters between early and hatched blastocysts. (**C**) FLIM image of the photon arrival times (right) of NAD(P)H and of FAD+ (left) showing variations in the metabolic state between the portion of the TE of a blastocyst inside and outside the zona pellucida. Color bars show the average photon arrival times in nanoseconds. (**D**) Of those embryos that were hatching (n = 36), we computed the ratio of the FLIM parameters of the TE between the inside and outside of the zona pellucida. The box plots depict the interquartile range of the ratio, the center of the box represents the mean, the horizontal line in the box represents the median and the vertical lines represent the 5 and 95% quartiles. Black dots represent data points outside of the interquartile range. Color dots represent the average ratio of each blastocyst. (**E**) FLIM parameters with largest separation between embryos of either Day 5 or 6 after fertilization were plotted in a 3D plot. Each dot corresponds to the mean of a single blastocyst. Support vector machine was used to create a hyperplane that best separates Day 5 (n = 98 from 71 patients) and Day 6 (n = 111 from 77 patients) blastocysts (gray plane). (**F**) We subdivided the data in four categories: Day 5 early/expanded (n = 47 from 41 patients), Day 5 hatching/hatched (n = 32 from 30 patients), Day 6 early/expanded (n = 51 from 39 patients) or Day 6 hatching/hatched (n = 79 from 58 patients) embryos. This box plot displays the standardized FLIM FAD+ short lifetime of these four categories, showing that both day and stage impact FAD+ short lifetime. (**G**) DAG of FAD+ short lifetime showing that embryo day and stage are correlated and that embryo FAD+ short lifetime is dependent both on embryo day and stage. Numbers in blue represent the coefficient of the multilevel model. Scale bars, 40 μm. *** signifies FDR $P < 0.001$, **FDR $P < 0.01$ and * signifies FDR $P < 0.05$. FAD+, flavine adenine dinucleotide; FLIM, fluorescence lifetime imaging microscopy; TE, trophectoderm.

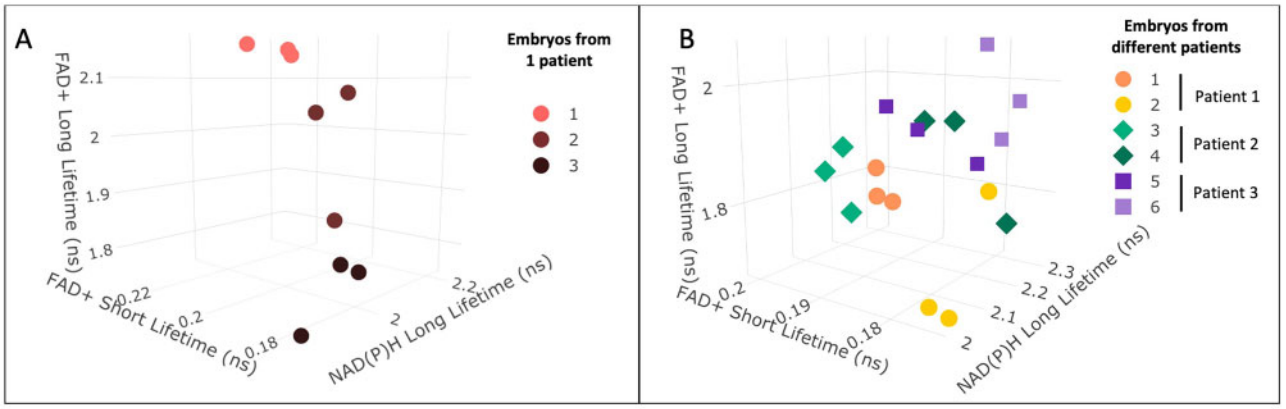

C Decomposition of variances between images within an embryo, embryos from the same patient, and different patients.

Level	NAD(P)H irradiance (a.u.)	NAD(P)H Fraction Engaged	NAD(P)H Long Lifetime(ns)	NAD(P)H Short Lifetime(ns)	FAD+ irradiance (a.u.)	FAD+ Fraction Engaged	FAD+ Long Lifetime(ns)	FAD+ Short Lifetime(ns)	Redox Ratio
	1.3×10^{-3}	4.4×10^{-5}	-	2.6×10^{-4}	1.6×10^{-2}	-	2.4×10^{-3}	7.4×10^{-5}	7.4×10^{-3}
	2.7×10^{-3}	11×10^{-5}	83×10^{-4}	8.6×10^{-4}	2.9×10^{-2}	36×10^{-5}	8.9×10^{-3}	18×10^{-5}	12×10^{-3}
	3.0×10^{-3}	8.6×10^{-5}	40×10^{-4}	3.0×10^{-4}	3.1×10^{-2}	5.3×10^{-5}	3.4×10^{-3}	3.5×10^{-5}	4.8×10^{-3}

D Percentage of variance explained by imaging depth, proportion of ICM photons vs TE, day of development, and developmental stage.

Level	NAD(P)H irradiance	NAD(P)H Fraction Engaged	NAD(P)H Long Lifetime	NAD(P)H Short Lifetime	FAD+ irradiance	FAD+ Fraction Engaged	FAD+ Long Lifetime	FAD+ Short Lifetime	Redox Ratio
	100%	0%	-	100%	100%	-	100%	100%	100%
	24%	0%	0%	0%	47%	42%	29%	0%	27%
	73%	0%	25%	26%	54%	0%	0%	0%	0%

Figure 4. Variance of the metabolic parameters between patients, embryos and images. Multilevel models encode information on the variance of each FLIM parameter between different patients, between different embryos from the same patient and between different images from the same embryo (taken at different Z positions). (**A**) Example of a patient with three different blastocysts. Colors correspond to a different embryo and each dot corresponds to a different image, from a different Z position, within the embryo. (**B**) Example of three patients with two embryos each imaged. Symbols correspond to different patients; each color corresponds to a different embryo and each dot corresponds to a different Z position within each embryo. (**C**) The variance of each FLIM parameter associated with each level: patient (top), embryo (middle) and images (bottom). FLIM parameter variances between patients were significantly different from 0 (FDR P-values ranging between 0.001 and 0.04), except NADH long lifetime and FAD+ fraction engaged. All variances associated with embryo level (FDR P-values ranging between 1.1×10^{-6} and 9×10^{-9}) and all variances between images within embryos were significantly different from 0 (P-values $< 1 \times 10^{-10}$). (**D**) The percentage of variance of each FLIM parameter associated with each level explained after controlling for embryo day, expansion stage, imaging depth and the proportion of photons coming from the ICM vs TE. About 100% corresponds to no statistically significant variance remaining after controlling for the listed factors. About 0% corresponds to the variances not being altered after controlling for the listed factors. FAD+, flavine adenine dinucleotide; FLIM, fluorescence lifetime imaging microscopy; ICM, inner cell mass; TE, trophectoderm.

patient. To more systematically quantify these effects, we used multilevel models (Snijders and Bosker, 2011; Lorah, 2018) to determine the residual variance in FLIM parameters explained by three levels: the differences between patients, between embryos from the same patient and between images taken at different Z positions of the same embryo (Fig. 4C). The residual variances of FLIM parameters for each level were significantly different than 0 (FDR $P > 0.05$), except for the variance of NADH Long Lifetime and FAD+ fraction engaged between patients. For the fluorescence lifetimes, the fractions engaged, and the redox ratio, the variance associated with differences between patients and between different Z positions were smaller than the variances associated with differences between embryos from the same patient.

We next investigated factors that might lead to the differences in FLIM parameters associated with these different levels (Fig. 4D).

Over 70% of the variance in NAD(P)H intensity and over 50% of the variance in FAD+ intensity between different *Z* positions of the same embryo can be explained by a combination of imaging depth and the proportion of photons coming from the ICM vs TE. Surprisingly, we found no association between FLIM parameters of blastocysts and maternal age at oocyte retrieval, patient BMI or levels of anti-Mullerian hormone (FDR $P > 0.05$), all of which are known to be associated with successful IVF outcome (Schoolcraft *et al.*, 1999; Moragianni *et al.*, 2012; Cimadomo *et al.*, 2018). Differences in FLIM parameters between patients were largely explained by differences in day of embryo development and expansion stage: after controlling for these two factors, NAD(P)H fraction engaged was the only FLIM parameter with statistically significant variance at the patient level. In contrast, there was still substantial variance in FLIM parameters between embryos from the same patient, even after controlling for day of embryo development, expansion stage, imaging depth and the proportion of photons coming from the ICM vs TE. Thus, there are metabolic difference between embryos from the same patient, which cannot be accounted for by these factors, and FLIM is sensitive enough to detect these metabolic differences.

Metabolic variations during human blastocyst expansion and hatching

The single timepoint FLIM measurements described above entail minimal exposure of the embryos to laser illumination and can be rapidly acquired, allowing us to obtain data on a large number of blastocysts. However, these measurements only provide information on the metabolic state of each blastocyst at one single instance in time. We next investigated the evolution of individual human blastocysts by performing continual time-lapse FLIM imaging.

To study the dynamic changes in metabolism during the expansion and hatching of preimplantation embryos, we performed time-lapse imaging of NAD(P)H (Fig. 5A), FAD+ (Fig. 5B, gray) and SHG (Fig. 5B, magenta) (Supplementary Video S2) of 10 morphologically normal human blastocysts from 10 different patients. We acquired three *Z*-planes for each channel every 2 h, over a 36-h period. To visualize the variations in metabolism of human blastocysts during development, we calculated the average photon arrival time of the segmented regions for both NAD(P)H (Fig. 5C) and FAD+ (Fig. 5D). Both signals showed complex spatial patterns, which evolved over time as the embryos progressed through development. The FLIM parameters showed continual metabolic variations over time during blastocyst development, with some parameters increasing and some decreasing as the embryos progressed past the early blastocyst stage (Fig. 5E).

The continual changes in FLIM parameters we observed with time-lapse imaging might reflect the endogenous evolution of blastocyst's metabolism or, alternatively, might be caused by artifacts due to the imaging procedure itself. To differentiate between these possibilities, we compared the results from time-lapse microscopy, in which embryos were on the microscopy and imaged for 36 h, to the results from the single timepoint FLIM measurements described above, in which each embryo was only subject to a single measurement. The differences between Days 5 and 6 embryos in the single time-point measurements provides a proxy for the endogenous evolution of blastocysts over 24 h, which we compared to the changes observed in time-lapse over a 24-h period (Supplementary Fig. S4A). NAD(P)H long lifetime, NAD(P)H short lifetime, and FAD+ irradiance, long lifetime, and short lifetime, exhibited statistically indistinguishable (FDR > 0.05) changes in both single timepoint and time-lapse imaging, arguing that these are due to the endogenous evolution of blastocyst's metabolism. However, NAD(P)H irradiance, NAD(P)H fraction engaged, and the redox ratio displayed significant differences (FDR $P < 0.05$), suggesting that these FLIM parameters are altered by the time-lapse imaging procedure. There are two possibilities, subtle metabolic changes could either be induced by light exposure during FLIM measurements or by the blastocysts being on the microscope stage for an extended period (instead of being in a standard incubator). To differentiate between these possibilities, we cultured seven human blastocysts on the microscope stage for 36 h subject only to individual FLIM measurements before and after the incubation period. We compared these blastocysts, which were not exposed to FLIM measurements during incubation to 10 human blastocysts that were subjected to FLIM measurements every 2 h for the 36-h incubation time. All FLIM parameters were statistically indistinguishable between the not exposed and the illuminated blastocysts (FDR $P > 0.05$, Supplementary Fig. S4B) and both sets of embryos progressed through development, as assessed by a senior embryologist. Thus, we conclude that light exposure during FLIM measurements (at the level investigated here) does not induce significant changes in FLIM parameters, but culturing blastocysts on the microscope stage for extended periods can cause subtle changes in embryo metabolism. Furthermore, there are continual, endogenous changes in blastocyst's metabolism that take place over the course of development.

Discussion

In this study, we explored the use of FLIM of NAD(P)H and FAD+ for measuring the metabolic state of human blastocysts. First, we studied 215 human blastocysts at a single timepoint, 2 h after thawing. We found that the metabolic state of these blastocysts varies based on both their time since fertilization and developmental stage. We also observed distinct metabolic states between cells in the ICM and the TE, and between cells inside and outside the zona pellucida. Using multilevel modeling of this data, we demonstrated that FLIM is sensitive enough to detect metabolic variations in individual blastocysts from the same patient and variations between patients. We next investigated the dynamics of blastocyst's metabolism using time-lapse FLIM imaging and found that the metabolic state of individual blastocysts change continuously over time.

Impaired metabolic activity results in decreased developmental capacity in oocytes and embryos, both in mouse (Wakefield *et al.*, 2011; Harvey, 2019) and human (Wilding *et al.*, 2001; Harvey, 2019). To this end, several reports have focused on detecting metabolic biomarkers of embryo quality (Gardner and Leese, 1987; Brison *et al.*, 2004; Dumollard *et al.*, 2007; Vergouw *et al.*, 2008; Heikal, 2010; Gardner *et al.*, 2011; Gardner and Harvey, 2015; Harvey, 2019). In this study, we have demonstrated the use of FLIM imaging to detect the metabolic state of human discarded blastocysts. We observed that combining FLIM with SHG imaging (Campagnola and Loew, 2003; Hsieh *et al.*, 2008; Yu *et al.*, 2014) provides information on a range of cellular and subcellular structures in human blastocysts, including

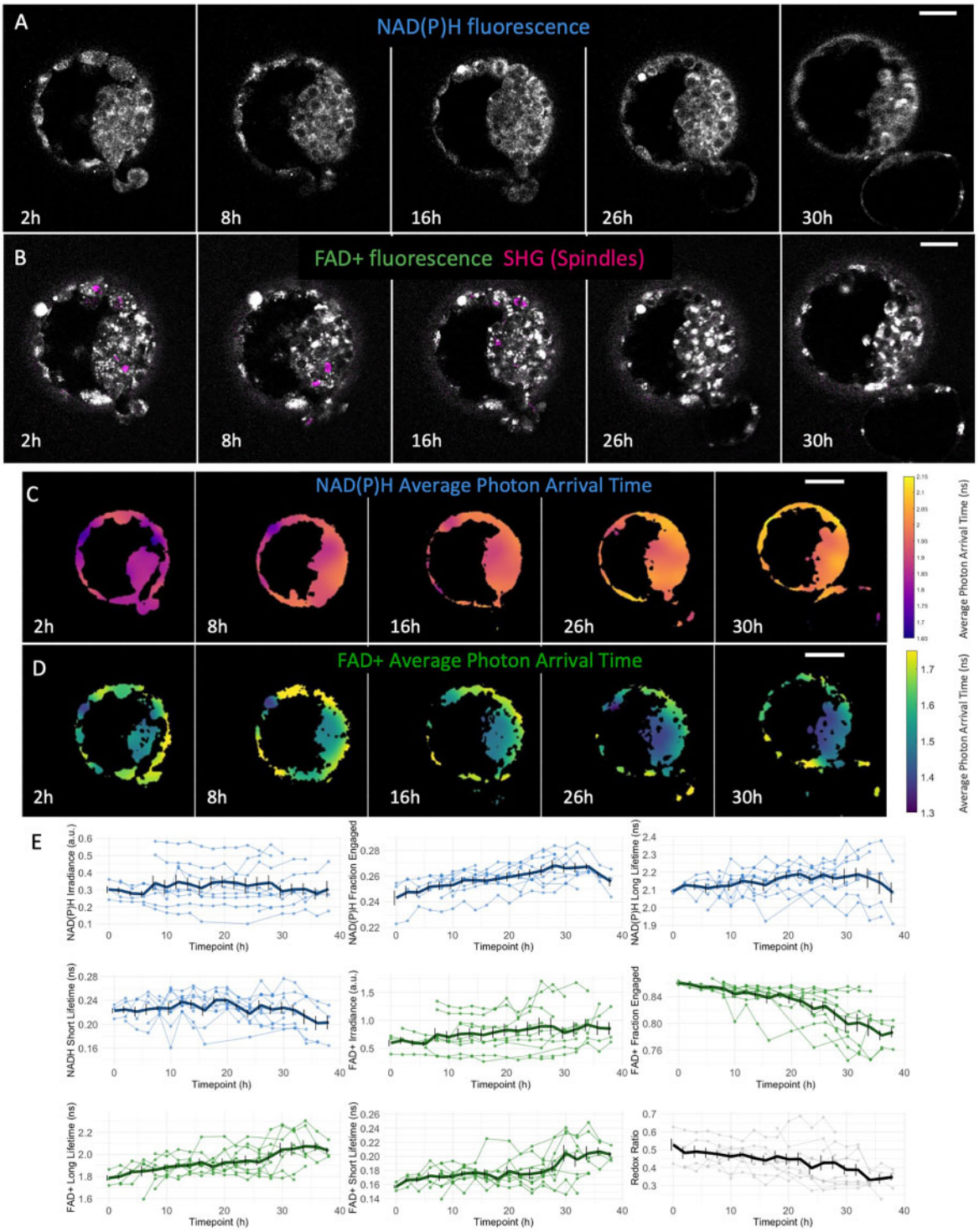

Figure 5. Non-invasive FLIM and SHG imaging detect metabolic variations during human blastocyst development. FLIM time-lapse imaging of the autofluorescence of NAD(P)H (**A**), and (**B**) of FAD+ (in gray) and SHG-spindle imaging (in magenta) of a human blastocyst throughout 36 h of incubation. (**C**) FLIM time-lapse imaging of the photon arrival times of NAD(P)H and (**D**) of FAD+ enable visualization of variations of metabolic state of human blastocysts throughout expansion and hatching. Color bars show the average photon arrival times in nanoseconds (also Supplementary Video S2). (**E**) Time trajectory plots of individual embryos (n = 10 from 10 patients) of four of the metabolic parameters produced. The average time curves from all the embryos are shown in thicker lines with SE bars, showing that these trends were reproducible among blastocysts. Scale bars, 40 μm. FAD+, flavine adenine dinucleotide; FLIM, fluorescence lifetime imaging microscopy; SHG, second-harmonic generation.

mitochondrial localization and physiology, spindle dynamics and mitotic divisions. Taken together, these results demonstrate that FLIM and SHG imaging can be used to obtain quantitative, non-invasive and biologically relevant information on live human blastocysts.

Metabolic shifts from the morula to the blastocyst stage have been described previously (Gardner *et al.*, 2001; Leese, 2012, 2015; Thompson *et al.*, 2016), including changes in redox state, and increasing levels of glucose uptake, oxygen consumption and lactate production (Houghton *et al.*, 1996; Trimarchi *et al.*, 2000; Harvey *et al.*, 2002; Gardner, 2015). Our results extend these prior reports by showing continuous variations in metabolic state during human blastocyst development from the early blastocyst to hatching stages. These results are in line with previously reported dynamic changes in embryo metabolism throughout development (Leese, 2002; Gardner and Harvey, 2015; Thompson *et al.*, 2016). In contrast with previous reports (Pais *et al.*, 2020), we observed highly significantly different metabolic states in human blastocysts at Day 5 vs Day 6 post fertilization. Human embryos develop at different rates, and our results show that only a fraction of the metabolic differences between blastocysts at different days post-fertilization can be explained by embryos tending to be at later developmental stages at later times. This implies an association between embryo developmental rate and metabolism, as has also been seen by other approaches (Leese, 2002; Gardner *et al.*, 2011; Santos Monteiro *et al.*, 2021). Taken together, these observations argue that the metabolism of human blastocysts is highly dynamic and flexible. It is an exciting future challenge to unravel the mechanistic basis of these metabolic variations in human embryos.

Our single timepoint measurements showing different metabolic states of cells in the ICM and TE are consistent with prior work indicating that they contain distinct mitochondrial physiology and function (Hewitson and Leese, 1993; Houghton, 2006; Van Blerkom, 2011; Gardner and Harvey, 2015). Thus, FLIM is sensitive enough to detect physiologically relevant changes in metabolism in human blastocysts, as has been previously seen for differentiation in *Caenorhabditis elegans* (Stringari *et al.*, 2011) and mouse neuronal development (Stringari *et al.*, 2012). We also observed differences in the metabolic state of TE cells inside and outside of the zona pellucida during hatching. To our knowledge, this has not been reported previously. There seem to be two possibilities: (i) these metabolic differences may reflect differing microenvironments. Perhaps the increase in lactate production, release and associated pH change in the surroundings, observed during hatching (Gardner, 2015), results from the different energy expenditure needed by TE cells inside vs outside the zona pellucida; or reflects embryo plasticity to adapt to the culture media (de Lima *et al.*, 2020); (ii) the hatching process itself may also lead to metabolic changes, either due to specific signaling pathways or a general response to associated stresses (Brison *et al.*, 2004). Future studies are planned to understand the nature of these variations.

In addition, by analyzing our data using multilevel modeling (Snijders and Bosker, 2011; Lorah, 2018), we found that blastocysts from the same patient have significantly different metabolic states. While some of this variation can be accounted for by time post fertilization and stage of development, a substantial variance between embryos remains even after accounting for these factors. It is unclear what causes these additional variations in metabolism between embryos. One possibility is that metabolism adjusts to respond to cellular or DNA damage, which are prevalent in preimplantation human embryos (Leese, 2002; Baumann *et al.*, 2007; Sturmey *et al.*, 2008). This provides an attractive explanation for the previously observed associations between blastocyst metabolism and viability (Gardner and Leese, 1987; Van Blerkom *et al.*, 1995; Gardner *et al.*, 2011). However, while embryo morphological scores are also associated with viability (Conaghan *et al.*, 1993; Schoolcraft *et al.*, 1999; Racowsky *et al.*, 2003; Ahlström *et al.*, 2011), we found no association between embryo metabolic state and morphological scores. This implies that multiple distinct processes impact embryo viability, some of which are associated with metabolism and others of which are associated with morphology. It will be of both fundamental interest and potential clinical import for future work to disentangle the contribution of specific pathways to embryo viability. Furthermore, the lack of association between metabolic state and morphology scores suggests that FLIM might provide synergistic information with conventional microscopy to aid in selecting the highest quality embryo for transfer in ART.

We found that FLIM illumination exposure during imaging did not induce significant changes in FLIM parameters but, culturing blastocysts on a FLIM microscope stage for extended periods can cause subtle variations in embryo metabolism. Thus, the on-stage microscope incubator and conventional incubator used in this study are not identical, though embryos successfully developed in both incubators. This highlights the need to critically evaluate the impact of on-stage microscope incubators, as has been previously pointed out in the context of conventional time-lapse imaging of embryos (Racowsky and Martins, 2017).

This study demonstrates that FLIM is sensitive enough to detect endogenous variations in the metabolism of discarded human blastocysts, which suggests its promise as a research tool and as a potential means to aid in embryo selection. Before FLIM is used on human embryos that will be transferred back to patients, it will be crucial to perform extensive additional safety studies. Prior work has shown that FLIM imaging does not appear to disrupt the development or viability of mouse embryos (Sanchez *et al.*, 2018; Seidler *et al.*, 2020) and mouse embryos exposed to FLIM illumination do not show higher rates of reactive oxygen species than non-illuminated control (Sanchez *et al.*, 2018). However, the results of safety studies in mice do not necessarily generalize to humans, so further studies focused on determining the impact of FLIM on human embryos are required.

There are also limitations to this study. First, the human blastocysts analyzed were vitrified, thawed and warmed for 2 h prior to FLIM imaging. Whether vitrification causes metabolic distress in human blastocysts remains unknown, even though its clinical success has been well documented (Rienzi *et al.*, 2017). In addition, it does not seem to alter mitochondrial potential or intracellular reactive oxygen species (Nohales-Córcoles *et al.*, 2016). Additionally, the blastocysts used in this study were discarded material, and include both euploid and aneuploid embryos. Our preliminary analysis indicates some associations between embryo metabolic state and ploidy (Shah *et al.*, 2020), which will be reported on in a subsequent manuscript. Future studies should focus on addressing this important subject in more detail. Surprisingly, we did not observe a correlation between blastocyst metabolic state and maternal age or BMI, each of which have long been linked with embryo quality (Schoolcraft *et al.*, 1999; Moragianni *et al.*, 2012) and mitochondrial function (Leary *et al.*, 2015; Morimoto *et al.*, 2020). This result must be interpreted with caution as it may reflect a selection bias in the material used in this study: we only imaged embryos that

were discarded, yet also reached the blastocyst stage. A clinical study using non-discarded embryos of all preimplantation developmental stages would provide a more complete view of the effect of maternal characteristics on embryo metabolic state. Finally, recent work has established a framework to relate FLIM parameters in oocytes to mitochondrial metabolic fluxes (Yang *et al.*, 2021), but additional work is required to determine if this is applicable to the later stage embryos studied here.

In summary, non-invasive metabolic imaging via FLIM is a promising tool for quantitatively characterizing the metabolic state of human blastocysts. FLIM can sensitively detected metabolic variations associated with blastocyst development over 36 h, the time post fertilization and blastocyst developmental stage. FLIM revealed differences in metabolic state between cells in the ICM and the TE, and between TE cells inside and outside the zona pellucida. The lack of an association between the metabolic state of human blastocyst and their morphological grading indicates that these two assessments may provide synergistic information to improve blastocyst selection. However, future work is required to determine the extent to which FLIM measurements are associated with the probability that a transferred human blastocyst will lead to a live birth.

Supplementary data

Supplementary data are available at *Human Reproduction* online.

Data availability

The data underlying this article will be shared on reasonable request to the corresponding author.

Acknowledgments

We would like to acknowledge Becker and Hickl GmbH and Boston Electronics for the loaning of electronic equipment for this research. We also acknowledge the Boston IVF embryologists and clinicians for their assistance during the project, in particular Dr Emily Seidler and Dr Alan Penzias and the Needleman lab, at Harvard University especially Brian Leahy, PhD, for useful advice.

Authors' roles

M.V. contributed to the conceptualization of the idea of the experiment, contributed to data acquisition, analysis, and interpretation, and drafted the manuscript. J.S.S. contributed to data acquisition and critical revision of the manuscript. X.Y. contributed to data analysis and interpretation of the results and critical revision of the manuscript. T.H.S. contributed to the conceptualization of the idea of the experiment and critical revision of the manuscript. W.C. contributed to data analysis and critical revision of the manuscript. D.S. contributed to the conceptualization of the idea of the experiment and interpretation of the results and critical revision of the manuscript. D.J.N. contributed to the conceptualization of the idea of the experiment and interpretation of the results and critical revision of the manuscript.

Funding

Supported by the Blavatnik Biomedical Accelerator Grant at Harvard University. Becker and Hickl GmbH and Boston Electronics sponsored research with the loaning of equipment for FLIM.

Conflict of interest

D.J.N. is an inventor on patent US20170039415A1.

References

Ahlström A, Westin C, Reismer E, Wikland M, Hardarson T. Trophectoderm morphology: an important parameter for predicting live birth after single blastocyst transfer. *Hum Reprod* 2011;**26**:3289–3296.

Ahlström A, Westin C, Wikland M, Hardarson T. Prediction of live birth in frozen–thawed single blastocyst transfer cycles by pre-freeze and post-thaw morphology. *Hum Reprod* 2013;**28**:1199–1209.

Alm H, Torner H, Löhrke B, Viergutz T, Ghoneim IM, Kanitz W. Bovine blastocyst development rate in vitro is influenced by selection of oocytes by brillant cresyl blue staining before IVM as indicator for glucose-6-phosphate dehydrogenase activity. *Theriogenology* 2005;**63**:2194–2205.

Al-Zubaidi U, Liu J, Cinar O, Robker RL, Adhikari D, Carroll J. The spatio-temporal dynamics of mitochondrial membrane potential during oocyte maturation. *Mol Hum Reprod* 2019;**25**:695–705.

Baumann CG, Morris DG, Sreenan JM, Leese HJ. The quiet embryo hypothesis: molecular characteristics favoring viability. *Mol Reprod Dev* 2007;**74**:1345–1353.

Becker W. *Advanced Time-Correlated Single Photon Counting Techniques*. 2005. https://link.springer.com/book/10.1007/3-540-28882-1 (1 December 2021, date last accessed).

Becker W. Fluorescence lifetime imaging—techniques and applications. *J Microsc* 2012;**247**:119–136.

Berg S, Kutra D, Kroeger T, Straehle CN, Kausler BX, Haubold C, Schiegg M, Ales J, Beier T, Rudy M *et al.* ilastik: interactive machine learning for (bio)image analysis. *Nat Methods* 2019;**16**:1226–1232.

Brison DR, Houghton FD, Falconer D, Roberts SA, Hawkhead J, Humpherson PG, Lieberman BA, Leese HJ. Identification of viable embryos in IVF by non-invasive measurement of amino acid turnover. *Hum Reprod* 2004;**19**:2319–2324.

Campagnola PJ, Loew LM. Second-harmonic imaging microscopy for visualizing biomolecular arrays in cells, tissues and organisms. *Nat Biotechnol* 2003;**21**:1356–1360.

Chi F, Sharpley MS, Nagaraj R, Roy SS, Banerjee U. Glycolysis-independent glucose metabolism distinguishes TE from ICM fate during mammalian embryogenesis. *Dev Cell* 2020;**53**:9–26.e4.

Cimadomo D, Fabozzi G, Vaiarelli A, Ubaldi N, Ubaldi FM, Rienzi L. Impact of maternal age on oocyte and embryo competence. *Front Endocrinol (Lausanne)*. 2018;**9**:327.

Cinco R, Digman MA, Gratton E, Luderer U. Spatial characterization of bioenergetics and metabolism of primordial to preovulatory follicles in whole ex vivo murine ovary. *Biol Reprod* 2016;**95**:129.

Conaghan J, Hardy K, Handyside AH, Winston RM, Leese HJ. Selection criteria for human embryo transfer: a comparison of pyruvate uptake and morphology. *J Assist Reprod Genet* 1993;**10**: 21–30.

Coticchio G, Mignini Renzini M, Novara PV, Lain M, De Ponti E, Turchi D, Fadini R, Dal Canto M. Focused time-lapse analysis reveals novel aspects of human fertilization and suggests new parameters of embryo viability. *Hum Reprod* 2018;**33**:23–31.

Cristianini N, Shawe-Taylor J. *An Introduction to Support Vector Machines: And Other Kernel-Based Learning Methods*. USA: Cambridge University Press, 1999.

Dumollard R, Carroll J, Duchen MR, Campbell K, Swann K. Mitochondrial function and redox state in mammalian embryos. *Semin Cell Dev Biol* 2009;**20**:346–353.

Dumollard R, Marangos P, Fitzharris G, Swann K, Duchen M, Carroll J. Sperm-triggered [Ca2+] oscillations and Ca2+ homeostasis in the mouse egg have an absolute requirement for mitochondrial ATP production. *Development* 2004;**131**:3057–3067.

Dumollard R, Ward Z, Carroll J, Duchen MR. Regulation of redox metabolism in the mouse oocyte and embryo. *Development* 2007; **134**:455–465.

Gardner DK. Lactate production by the mammalian blastocyst: manipulating the microenvironment for uterine implantation and invasion? *Bioessays* 2015;**37**:364–371.

Gardner DK, Harvey AJ. Blastocyst metabolism. *Reprod Fertil Dev* 2015;**27**:638–654.

Gardner DK, Lane M, Stevens J, Schlenker T, Schoolcraft WB. Blastocyst score affects implantation and pregnancy outcome: towards a single blastocyst transfer. *Fertil Steril* 2000;**73**:1155–1158.

Gardner DK, Lane M, Stevens J, Schoolcraft WB. Noninvasive assessment of human embryo nutrient consumption as a measure of developmental potential. *Fertil Steril* 2001;**76**:1175–1180.

Gardner DK, Leese HJ. Assessment of embryo viability prior to transfer by the noninvasive measurement of glucose uptake. *J Exp Zool* 1987;**242**:103–105.

Gardner DK, Wale PL, Collins R, Lane M. Glucose consumption of single post-compaction human embryos is predictive of embryo sex and live birth outcome. *Hum Reprod* 2011;**26**:1981–1986.

Gerris J, De Sutter P, De Neubourg D, Van Royen E, Vander Elst J, Mangelschots K, Vercruyssen M, Kok P, Elseviers M, Annemans L *et al*. A real-life prospective health economic study of elective single embryo transfer versus two-embryo transfer in first IVF/ICSI cycles. *Hum Reprod* 2004;**19**:917–923.

Ghukasyan VV, Heikal AA. *Natural Biomarkers for Cellular Metabolism: Biology, Techniques, and Applications*. Florida, USA: CRC Press, 2014.

Harvey AJ. Mitochondria in early development: linking the microenvironment, metabolism and the epigenome. *Reproduction* 2019;**157**: R159–R179.

Harvey AJ, Kind KL, Thompson JG. REDOX regulation of early embryo development. *Reproduction* 2002;**123**:479–486.

Heikal AA. Intracellular coenzymes as natural biomarkers for metabolic activities and mitochondrial anomalies. *Biomark Med* 2010;**4**: 241–263.

Hewitson LC, Leese HJ. Energy metabolism of the trophectoderm and inner cell mass of the mouse blastocyst. *J Exp Zool* 1993;**267**: 337–343.

Houghton FD. Energy metabolism of the inner cell mass and trophectoderm of the mouse blastocyst. *Differentiation* 2006;**74**: 11–18.

Houghton FD, Thompson JG, Kennedy CJ, Leese HJ. Oxygen consumption and energy metabolism of the early mouse embryo. *Mol Reprod Dev* 1996;**44**:476–485.

Hsieh C-S, Chen S-U, Lee Y-W, Yang Y-S, Sun C-K. Higher harmonic generation microscopy of in vitro cultured mammal oocytes and embryos. *Opt Express* 2008;**16**:11574–11588.

Jones GM, Trounson AO, Vella PJ, Thouas GA, Lolatgis N, Wood C. Glucose metabolism of human morula and blastocyst-stage embryos and its relationship to viability after transfer. *Reprod Biomed Online* 2001;**3**:124–132.

Klaidman LK, Leung AC, Adams JD. High-performance liquid chromatography analysis of oxidized and reduced pyridine dinucleotides in specific brain regions. *Anal Biochem* 1995;**228**:312–317.

Leary C, Leese HJ, Sturmey RG. Human embryos from overweight and obese women display phenotypic and metabolic abnormalities. *Hum Reprod* 2015;**30**:122–132.

Leese HJ. Quiet please, do not disturb: a hypothesis of embryo metabolism and viability. *Bioessays* 2002;**24**:845–849.

Leese HJ. Metabolism of the preimplantation embryo: 40 years on. *Reproduction* 2012;**143**:417–427.

Leese HJ. History of oocyte and embryo metabolism. *Reprod Fertil Dev* 2015;**27**:567–571.

Lima C. D, Santos É. D, Ispada J, Fontes PK, Nogueira MFG, Santos C. D, Milazzotto MP. The dynamics between in vitro culture and metabolism: embryonic adaptation to environmental changes. *Sci Rep* 2020;**10**:15672.

Lopes AS, Lane M, Thompson JG. Oxygen consumption and ROS production are increased at the time of fertilization and cell cleavage in bovine zygotes. *Hum Reprod* 2010;**25**:2762–2773.

Lorah J. Effect size measures for multilevel models: definition, interpretation, and TIMSS example. *Large Scale Assess Educ* 2018;**6**:8.

Ma N, Mochel N. D, Pham PD, Yoo TY, Cho KWY, Digman MA. Label-free assessment of pre-implantation embryo quality by the Fluorescence Lifetime Imaging Microscopy (FLIM)-phasor approach. *Sci Rep* 2019;**9**:13206.

Mertz J. *Introduction to Optical Microscopy*. *Higher Education from Cambridge University Press*. 2019. https://www.cambridge.org/highereducation/books/introduction-to-optical-microscopy/F6C6318C87732519D7E07BA7A03F0B81 (26 April 2021, date last accessed).

Moragianni VA, Jones S-ML, Ryley DA. The effect of body mass index on the outcomes of first assisted reproductive technology cycles. *Fertil Steril* 2012;**98**:102–108.

Morimoto N, Hashimoto S, Yamanaka M, Nakano T, Satoh M, Nakaoka Y, Iwata H, Fukui A, Morimoto Y, Shibahara H. Mitochondrial oxygen consumption rate of human embryos declines with maternal age. *J Assist Reprod Genet* 2020;**37**: 1815–1821.

Munné S, Kaplan B, Frattarelli JL, Child T, Nakhuda G, Shamma FN, Silverberg K, Kalista T, Handyside AH, Katz-Jaffe M *et al.*; STAR Study Group. Preimplantation genetic testing for aneuploidy versus morphology as selection criteria for single frozen-thawed embryo transfer in good-prognosis patients: a multicenter randomized clinical trial. *Fertil Steril* 2019;**112**:1071–1079.e7.

Neapolitan RE. *Probabilistic Methods for Bioinformatics*. 2009 https://www.elsevier.com/books/probabilistic-methods-for-bioinformatics/neapolitan/978-0-12-370476-4 (1 February 2021, date last accessed).

Nohales-Córcoles M, Sevillano-Almerich G, Di Emidio G, Tatone C, Cobo AC, Dumollard R, De Los Santos Molina MJ. Impact of vitrification on the mitochondrial activity and redox homeostasis of human oocyte. *Hum Reprod* 2016;**31**:1850–1858.

Pais RJ, Sharara F, Zmuidinaite R, Butler S, Keshavarz S, Iles R. Bioinformatic identification of euploid and aneuploid embryo secretome signatures in IVF culture media based on MALDI-ToF mass spectrometry. *J Assist Reprod Genet* 2020;**37**:2189–2198.

Patrizio P, Shoham G, Shoham Z, Leong M, Barad DH, Gleicher N. Worldwide live births following the transfer of chromosomally "Abnormal" embryos after PGT/A: results of a worldwide web-based survey. *J Assist Reprod Genet* 2019;**36**:1599–1607.

Pearl J. *Causal Inference in Statistics: A Primer*. 2016. https://www.wiley.com/en-us/Causal+Inference+in+Statistics%3A+A+Primer-p-9781119186847 (1 October 2021, date last accessed).

Penzias A, Bendikson K, Butts S, Coutifaris C, Falcone T, Fossum G, Gitlin S, Gracia C, Hansen K, La Barbera A *et al*. The use of preimplantation genetic testing for aneuploidy (PGT-A): a committee opinion. *Fertil Steril* 2018;**109**:429–436.

Racowsky C, Combelles CMH, Nureddin A, Pan Y, Finn A, Miles L, Gale S, O'Leary T, Jackson KV. Day 3 and day 5 morphological predictors of embryo viability. *Reprod Biomed Online* 2003;**6**:323–331.

Racowsky C, Martins WP. Effectiveness and safety of time-lapse imaging for embryo culture and selection: it is still too early for any conclusions? *Fertil Steril* 2017;**108**:450–452.

Rienzi L, Gracia C, Maggiulli R, LaBarbera AR, Kaser DJ, Ubaldi FM, Vanderpoel S, Racowsky C. Oocyte, embryo and blastocyst cryopreservation in ART: systematic review and meta-analysis comparing slow-freezing versus vitrification to produce evidence for the development of global guidance. *Hum Reprod Update* 2017;**23**:139–155.

Saha B, Ganguly A, Home P, Bhattacharya B, Ray S, Ghosh A, Rumi MAK, Marsh C, French VA, Gunewardena S *et al*. TEAD4 ensures postimplantation development by promoting trophoblast self-renewal: An implication in early human pregnancy loss. *Proc Natl Acad Sci USA* 2020;**117**:17864–17875.

Sanchez T, Venturas M, Aghvami SA, Yang X, Fraden S, Sakkas D, Needleman DJ. Combined noninvasive metabolic and spindle imaging as potential tools for embryo and oocyte assessment. *Hum Reprod* 2019;**34**:2349–2361.

Sanchez T, Wang T, Pedro MV, Zhang M, Esencan E, Sakkas D, Needleman D, Seli E. Metabolic imaging with the use of fluorescence lifetime imaging microscopy (FLIM) accurately detects mitochondrial dysfunction in mouse oocytes. *Fertil Steril* 2018;**110**:1387–1397.

Santos Monteiro CA, Chow DJX, Leal GR, Tan TC, Reis Ferreira AM, Thompson JG, Dunning KR. Optical imaging of cleavage stage bovine embryos using hyperspectral and confocal approaches reveals metabolic differences between on-time and fast-developing embryos. *Theriogenology* 2021;**159**:60–68.

Schoolcraft WB, Gardner DK, Lane M, Schlenker T, Hamilton F, Meldrum DR. Blastocyst culture and transfer: analysis of results and parameters affecting outcome in two in vitro fertilization programs. *Fertil Steril* 1999;**72**:604–609.

Seidler EA, Sanchez T, Venturas M, Sakkas D, Needleman DJ. Noninvasive imaging of mouse embryo metabolism in response to induced hypoxia. *J Assist Reprod Genet* 2020;**37**:1797–1805.

Seli E, Sakkas D, Scott R, Kwok SC, Rosendahl SM, Burns DH. Noninvasive metabolomic profiling of embryo culture media using Raman and near-infrared spectroscopy correlates with reproductive potential of embryos in women undergoing in vitro fertilization. *Fertil Steril* 2007;**88**:1350–1357.

Shah JS, Venturas M, Sanchez TH, Penzias AS, Needleman D, Sakkas D. Fluorescence lifetime imaging microscopy (FLIM) detects differences in metabolic signatures between euploid and aneuploid human blastocysts. *Fertil Steril* 2020;**114**:e76–e77.

Snijders TAB, Bosker RJ. *Multilevel Analysis: An Introduction to Basic and Advanced Multilevel Modeling*. London: SAGE, 2011.

Stringari C, Cinquin A, Cinquin O, Digman MA, Donovan PJ, Gratton E. Phasor approach to fluorescence lifetime microscopy distinguishes different metabolic states of germ cells in a live tissue. *Proc Natl Acad Sci USA* 2011;**108**:13582–13587.

Stringari C, Nourse JL, Flanagan LA, Gratton E. Phasor fluorescence lifetime microscopy of free and protein-bound NADH reveals neural stem cell differentiation potential. *PLoS One* 2012;**7**:e48014.

Sturmey RG, Brison DR, Leese HJ. Symposium: innovative techniques in human embryo viability assessment. Assessing embryo viability by measurement of amino acid turnover. *Reprod Biomed Online* 2008;**17**:486–496.

Sutton-McDowall ML, Gosnell M, Anwer AG, White M, Purdey M, Abell AD, Goldys EM, Thompson JG. Hyperspectral microscopy can detect metabolic heterogeneity within bovine post-compaction embryos incubated under two oxygen concentrations (7% versus 20%). *Hum Reprod* 2017;**32**:2016–2025.

Tejera A, Herrero J, Viloria T, Romero JL, Gamiz P, Meseguer M. Time-dependent O2 consumption patterns determined optimal time ranges for selecting viable human embryos. *Fertil Steril* 2012;**98**:849–857.e3.

Thompson JG, Brown HM, Sutton-McDowall ML. Measuring embryo metabolism to predict embryo quality. *Reprod Fertil Dev* 2016;**28**:41–50.

Tran D, Cooke S, Illingworth PJ, Gardner DK. Deep learning as a predictive tool for fetal heart pregnancy following time-lapse incubation and blastocyst transfer. *Hum Reprod* 2019;**34**:1011–1018.

Trimarchi JR, Liu L, Porterfield DM, Smith PJS, Keefe DL. Oxidative phosphorylation-dependent and -independent oxygen consumption by individual preimplantation mouse embryos1. *Biol Reprod* 2000;**62**:1866–1874.

Turner K, Martin KL, Woodward BJ, Lenton EA, Leese HJ. Comparison of pyruvate uptake by embryos derived from conception and non-conception natural cycles. *Hum Reprod* 1994;**9**:2362–2366.

Urbanski JP, Johnson MT, Craig DD, Potter DL, Gardner DK, Thorsen T. Noninvasive metabolic profiling using microfluidics for analysis of single preimplantation embryos. *Anal Chem* 2008;**80**:6500–6507.

Van Blerkom J. Mitochondrial function in the human oocyte and embryo and their role in developmental competence. *Mitochondrion* 2011;**11**:797–813.

Van Blerkom J, Davis PW, Lee J. ATP content of human oocytes and developmental potential and outcome after in-vitro fertilization and embryo transfer. *Hum Reprod* 1995;**10**:415–424.

Vergouw CG, Botros LL, Roos P, Lens JW, Schats R, Hompes PGA, Burns DH, Lambalk CB. Metabolomic profiling by near-infrared spectroscopy as a tool to assess embryo viability: a novel, non-invasive method for embryo selection. *Hum Reprod* 2008;**23**: 1499–1504.

Wakefield SL, Lane M, Mitchell M. Impaired mitochondrial function in the preimplantation embryo perturbs fetal and placental development in the mouse. *Biol Reprod* 2011;**84**:572–580.

Wilding M, Dale B, Marino M, Matteo L. D, Alviggi C, Pisaturo ML, Lombardi L, De Placido G. Mitochondrial aggregation patterns and activity in human oocytes and preimplantation embryos. *Hum Reprod* 2001;**16**:909–917.

Wong KM, Repping S, Mastenbroek S. Limitations of embryo selection methods. *Semin Reprod Med* 2014;**32**:127–133.

Yang X, Ha G, Needleman DJ. A coarse-grained NADH redox model enables inference of subcellular metabolic fluxes from fluorescence lifetime imaging. *eLife* 2021;**10**:e73808.

Yu C-H, Langowitz N, Wu H-Y, Farhadifar R, Brugues J, Yoo TY, Needleman D. Measuring microtubule polarity in spindles with second-harmonic generation. *Biophys J* 2014;**106**:1578–1587.

Zhu M, Zernicka-Goetz M. Living a sweet life: glucose instructs cell fate in the mouse embryo. *Dev Cell* 2020;**53**:1–2.